Journal of Fluid Science and Technology

Vol. 7, No. 3, 2012

Backlayering Distance of Thermal Fumes in Tunnel Fire Experiments Using a Large-Scale Model*

Tomoya MINEHIRO**, Katsushi FUJITA***, Nobuyoshi KAWABATA****, Masato HASEGAWA**** and Futoshi TANAKA*****

**Graduate School of Natural Science and Technology, Kanazawa University, Kakuma-machi, Kanazawa-shi, Ishikawa 920-1192, JAPAN
E-mail: minehiro@stu.kanazawa-u.ac.jp

***Department of Mechanical Engineering, Fukui National College of Technology, Geshi-cho, Sabae-shi, Fukui 916-8507, JAPAN
E-mail: fujita@fukui-nct.ac.jp

****School of Mechanical Engineering, Kanazawa University, Kakuma-machi, Kanazawa-shi, Ishikawa 920-1192, JAPAN
E-mail: kwbt@t.kanazawa-u.ac.jp, mhase@t.kanazawa-u.ac.jp

*****Department of Mechanical Engineering, University of Fukui, 3-9-1 Bunkyo, Fukui-shi, Fukui 910-8507, JAPAN
E-mail: f-tanaka@u-fukui.ac.jp

Abstract

In this study, the backlayering distance of thermal fumes in a tunnel fire was examined by using a large-scale model tunnel. A 1/5-scale model was constructed taking into consideration both the similarity of thermal characteristics in the wall and Froude similarity. Experimental parameters were the heat release rate of the fire source and the longitudinal ventilation velocity. The following conclusions were obtained. A new expression was proposed to calculate the dimensionless backlayering distance based on the dimensionless heat release rate and Froude number. Constants included in this expression were obtained from experimental data by using the least-squares method. The backlayering distance calculated by the new expression was compared with that calculated by previous expressions developed by other researchers. The new expression has the ability to calculate not only the backlayering distance but also the critical velocity.

Key words: Turbulent Flow, Flow Measurements, Stratified Flow, Backlayering Distance, Tunnel Fire, Thermal Fumes, Model Experiment

1. Introduction

In Japan, road tunnels are constructed not only in mountainous areas but also in urban centers in line with the development of the expressway network. These expressway road tunnels are generally unidirectional and adopt longitudinal ventilation, which blows parallel to the direction of passing vehicles. In the event of a fire in a one-way tunnel, a traffic jam is created on the upstream side of the fire, and drivers and passengers must be evacuated from vehicles inside the tunnel. In such a situation, the most important consideration in tunnel design is maintaining an environment which is safe for evacuees, fire fighters, and rescue workers.

Emergency ventilation measures for a one-way tunnel using a longitudinal ventilation system are as follows. Ventilation wind prevents the backlayering of thermal fumes, which flow against the wind of longitudinal ventilation, in the upstream direction from a fire.

*Received 14 Aug., 2012 (No. T2-10-0454)
Japanese Original : Trans. Jpn. Soc. Mech. Eng., Vol.77, No.776, B (2011), pp.1064-1074 (Received 14 June, 2010)
[DOI: 10.1299/jfst.7.389]

Thermal fumes are swept away in the downstream direction from a fire. As a result, a secure environment is maintained on the upstream side. It is essential to grasp the characteristics of the backlayering thermal fumes in the case of a tunnel fire.

In research on the backlayering flow phenomenon in a tunnel fire, the critical velocity for preventing backlayering thermal fumes has been extensively studied using a number of methods: theory analysis[1],[2], fire experiments[3]-[8], and numerical simulation[9],[10]. On the other hand, the backlayering distance of the thermal fumes, which flow under the tunnel ceiling against the wind of the longitudinal ventilation, is also an important characteristic. Approaches to studying the backlayering distance include model experiments[5],[11]-[13], numerical simulation[13],[14], and an expression to calculate the backlayering distance by theoretical analysis[15],[16]. However, compared to research on the critical velocity, there have been few studies on the backlayering distance. A parametric study using a wide range of heat release rates and longitudinal ventilation velocities is required.

Previously, we studied the flow phenomenon of thermal fumes based on the temperature distribution inside the tunnel[17]. In the present paper, in addition to the critical velocity, we report the backlayering distance of the thermal fumes as one of the backlayering characteristics of thermal fumes in a tunnel fire. Tunnel fire experiments were conducted using a large-scale model, and a new expression was proposed to calculate the dimensionless backlayering distance based on the dimensionless heat release rate and Froude number. The new expression can determine not only the backlayering distance but also the critical velocity.

2. Nomenclature

A : Cross sectional area of tunnel [m^2]
As : Aspect ratio $As = B/H$ [-]
B : Width of tunnel [m]
Bi : Biot number [-] $Bi = hH/\lambda$
Fo : Fourier number [-] $Fo = \alpha\sqrt{H/g}\,/H^2$
Fr : Froude number $Fr = U_s/\sqrt{gH}$ [-]
g : Gravitational acceleration [m/s^2]
H : Height of tunnel (characteristic length) [m]
h : Heat-transfer coefficient [W/m^{2}K]
L_b : Backlayering distance of thermal fumes [m]
Q : Instantaneous heat release rate [W]
Q_m : Average quasi-steady heat release rate [W]
Q_s : Quasi-steady heat release rate [W]
Q^*_m : Dimensionless average quasi-steady heat release rate $Q^* = Q_m / (\rho_0 C_p T_0 A \sqrt{gH})$ [-]
Re : Reynolds number $Re = U_s H/\nu$ [-]
T_0 : Ambient temperature [K]
U : Instantaneous velocity of longitudinal ventilation [m/s]
U_s : Average velocity of longitudinal ventilation (characteristic velocity) [m/s]
δT : Temperature rise [K]
δT^* : Dimensionless temperature rise $\delta T^* = \delta T/T_0$ [-]
α : Thermal diffusivity [m^2/s]
λ : Thermal conductivity [W/mK]
γ : Scale ratio [-]
ν : Kinematic viscosity [m^2/s]

ρ_0 : Air density at ambient temperature [kg/m^3]

3. Experimental equipment and measurement methods

3.1 Model tunnel

Figure 1 shows the experimental equipment of the large-scale model tunnel, which is basically the same as used in our previous study[17]. The model tunnel is scaled down to 1/5 of the size of a full-scale tunnel. The origin of the coordinates is the position of the fire source. The size of the model tunnel is as follows: 41.4 m in total length (x-coordinate), 1.93 m in width (y-coordinate), and 1 m in height (z-coordinate). The cross section of the model tunnel is rectangular.

The heat release rate, temperature distribution, and wind velocity were measured similarly to the previous study[17]. The heat release rate was calculated from the burning rate of fuel measured by an electronic balance[18] and the amount of radiant heat flux of fire was measured by a radiometer[19]. The temperature inside the model tunnel was measured by thermocouples fixed at 297 points on the ceiling and the central longitudinal section of the model tunnel. K-type thermocouples of 0.1-mm diameter with a small time constant were used to measure the temperature distribution. The temperature was acquired at 1.0-s intervals. Thermocouples at 8 locations in the vertical direction of the tunnel were positioned at 2-m intervals in the central longitudinal section of the model tunnel. Thermocouples at 128 locations were installed in the central longitudinal section. Thermocouples at 9 locations in the width direction were installed at 2-m intervals under the ceiling of the model tunnel. These thermocouples were placed 20 mm directly below the ceiling. In addition, the thermocouples under the ceiling were installed in the central line (y = 0 m) at 1-m intervals. Thermocouples at 169 locations were installed under the ceiling. Laser units to visualize smoke fumes were positioned in two locations on the upstream side of the fire: x = 32 m, y = 0.15 and 0.65 m, z = 0.9 m. The laser unit irradiates laser beams parallel to the ceiling toward the fire source direction from the opening of the model tunnel.

3.2 Experimental conditions

The scale of the fire in the experiments was 65, 170, 240, and 390 kW (burning area of combustion vessel: 0.079, 0.15, 0.18, and 0.22 m^2), respectively. n-Heptane (lower heating value: 44.56 MJ/kg), which is the main ingredient of gasoline, was used as the fuel of the fire source. The longitudinal ventilation velocity was examined in the range from 0.61 to 1.67 m/s. In total, 39 fire experiments were conducted.

3.3 Longitudinal wind velocity

The longitudinal ventilation velocity through the model tunnel was measured by an anemometer as well as by using particle image velocimetry (PIV). The PIV method was used to verify the measurement accuracy of the anemometer in the range of low wind velocity of less than 1.0 m/s.

As shown in Fig. 1, the anemometers were placed in four locations on the upstream side of the fire in the model tunnel: x = 24.5 m, (y, z) = (0.5, 0.25 m), (0.5, 0.85 m), (−0.5, 0.25 m), (−0.5, 0.85 m). The wind velocity was acquired at 1.0-s intervals. A charge-coupled device (CCD) video camera was installed at one location on the upstream side of the fire: x = 25 m, z = 0.6 m. A window was installed in an outer wall of the model tunnel; the images for PIV were taken through the window at 0.01-s intervals using the CCD video camera from the exterior of the model tunnel. Sheet lighting was used for visualization inside the model tunnel. The coordinates of the source of the sheet lighting were x = 25 m, y = 0 m, and z = 0.0 m. Silica particles of 1.7-μm average diameter were used as tracer particles for PIV. The silica particles were scattered by the longitudinal wind from the upstream side of

the sheet lighting. Images were taken for 10 s as the initial condition before fire ignition, and then images for 5 s were taken every 90 s in the time range from ignition to extinguishing. The range of the image was from z = 0.4 to 0.85 m, and the width of the x direction was 0.55 m. The open-source PIV program (MatPIV) was used as the software for PIV analysis[20]. MatPIV is based on the cross-correlation method using the fast Fourier transform (FFT). The average value of all of the velocity vectors for 5 s was used as the value measured by the PIV method.

The upper parts of Figs. 2 and 3 show the time curves of the average value measured by the anemometers at four locations and the diamond-shape points measured by the PIV method as the velocity U of the longitudinal ventilation. The time curves of the velocity measured by the anemometers show a steady value after ignition, which is in agreement with the diamond-shape points measured by the PIV method. Therefore, the measurement accuracy of the anemometers was reliable in the range of low wind velocity of less than 1.0 m/s. Judging from this, the measurement result by the anemometers was used as the velocity of longitudinal wind through the model tunnel in a fire.

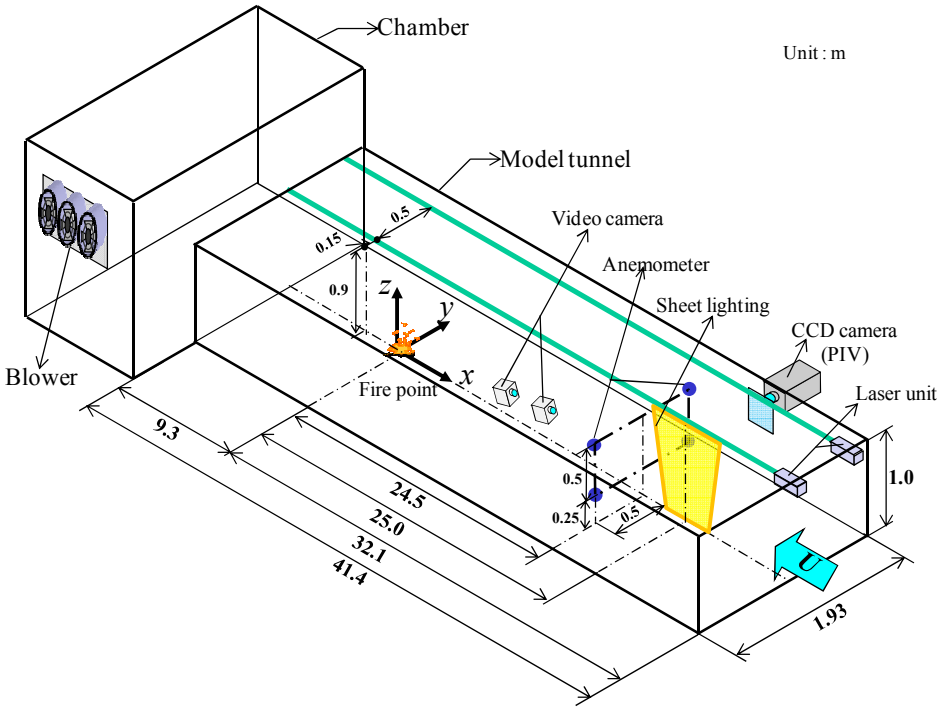

Fig. 1 Schematic diagram of the model tunnel

3.4 Quasi-steady condition

The lower parts of Figs. 2 and 3 show the time curves of the instantaneous heat release rate Q. The average value for 15 s of the instantaneous heat release rate is marked by a white circle. The time period during which the fluctuation of the average value is less than 5% was defined as the time period of a quasi-steady condition. This definition is basically the same as that in our previous paper[17]. The quasi-steady condition is shown as the time period between the dashed lines in the lower parts of Figs. 2 and 3. In the range of the experimental conditions of this research, the quasi-steady condition was maintained for 30 s or more in all of the experimental cases. Here, the quasi-steady heat release rate Q_s was defined as the average value of the last 30 s within the time period of the quasi-steady condition.

The upper parts of Figs. 2 and 3 show the time curves of the instantaneous velocity U of the longitudinal ventilation. The average velocity U_s of the longitudinal ventilation in the

same time period as the quasi-steady heat release rate was defined as the characteristic velocity. The difference between instantaneous velocity and the average velocity was defined as the fluctuation of the velocity of longitudinal ventilation. The fluctuation range for the time period of the quasi-steady condition was small: 5% or less of the average velocity.

The distance of the backlayering thermal fumes becomes the maximum distance for the time period of the quasi-steady condition in the lower parts of Figs. 2 and 3. The backlayering distance of the respective experiments was defined as the maximum value of the time curve of the backlayering distance.

When the size of the combustion vessel of the fire source was the same, the average value of the quasi-steady heat release rate of the respective experiments, which changed the average velocity of the longitudinal ventilation, was defined as the average heat release rate Q_m. The values of the average heat release rate were 66.2, 165.3, 229.4, and 377.4 kW (burning area of combustion vessel: 0.079, 0.15, 0.18, 0.22 m^2), respectively. These heat release rates are equivalent to a fire scale of 3.7, 9.3, 12.8, and 21.1 MW in a full-scale tunnel (scale ratio $\gamma = 5$). In the case of 3.7 and 21.1 MW, it is equivalent to one passenger vehicle and one bus on fire, respectively, as suggested by the PIARC Committee[21].

In the following sections, the discussion focuses on these parameters: average heat release rate Q_m, average velocity U_s of the longitudinal ventilation, and backlayering distance L_b.

3.5 Backlayering distance

Two methods were used to measure the backlayering distance L_b in our tunnel fire experiments. The first is a temperature distribution method using the thermocouples under the ceiling. The other method visualizes the tip position of the backlayering smoke by the laser beam from the laser units installed in locations on the upstream side of the fire. As shown in the schematic representation of Fig. 4, it was determined that the backlayering smoke can be visualized by the scattering of the laser beam. Several video cameras were installed on the floor of the model tunnel, and the tip position of the smoke fumes was calculated from the images captured by the video cameras.

Figure 5 shows the distribution of the temperature rise δT from the ambient temperature at the center of the tunnel ceiling. The distribution in four cases that changed the average heat release rate Q_m and the average velocity U_s of the longitudinal ventilation is shown in Fig. 5. The temperature rise δT increases rapidly at the tip position of the thermal fumes. The tip position does not change sharply even if the judgment value of the temperature rise δT changes: δT = 5, 10, and 30 K. From this figure, the tip position of the thermal fumes was defined as the position at which the temperature rise exceeds 5 K. Likewise, we defined the domain of the temperature rise above 5 K as the domain of the thermal fumes. The backlayering distance was defined as the distance from the tip position of the thermal fumes to the origin of the x-coordinate in this study.

The lower parts of Figs. 2 and 3 compares measurement results between the laser beam and temperature distribution methods. Apart from the case where the backlayering distance is less than one meter, the measurements obtained by the two methods are in reasonable agreement with each other. For the backlayering distance below one meter, the measurement accuracy of the temperature distribution method decreased due to the effect of radiant heat from the fire source. Accordingly, the laser beam method was used for measuring backlayering distance below three meters. The temperature distribution method was used to measure backlayering distance of three meters or more.

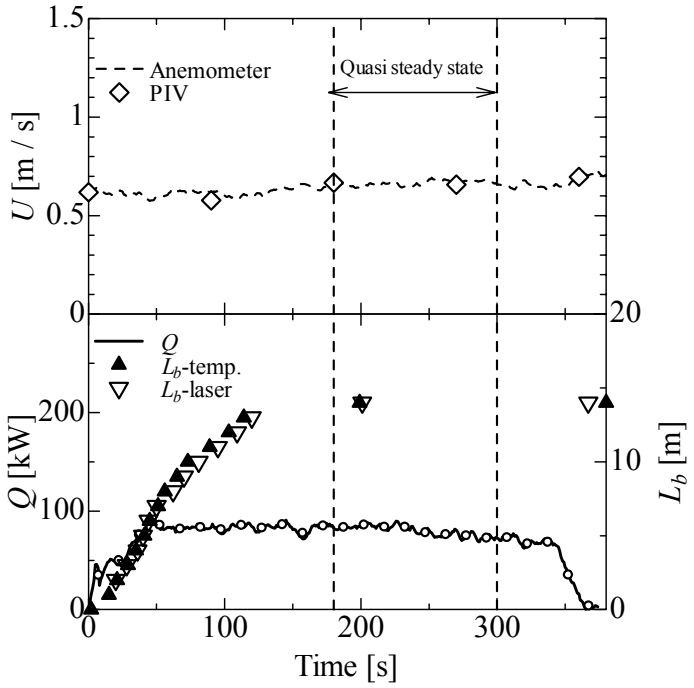

Fig. 2 Time curves of the heat release rate Q measured by electronic balance, ventilation velocity U measured by anemometer and PIV method, and backlayering distance L_b measured by temperature distribution and laser beam methods, in the case of a burning area of $A_f = 0.079$ m^2

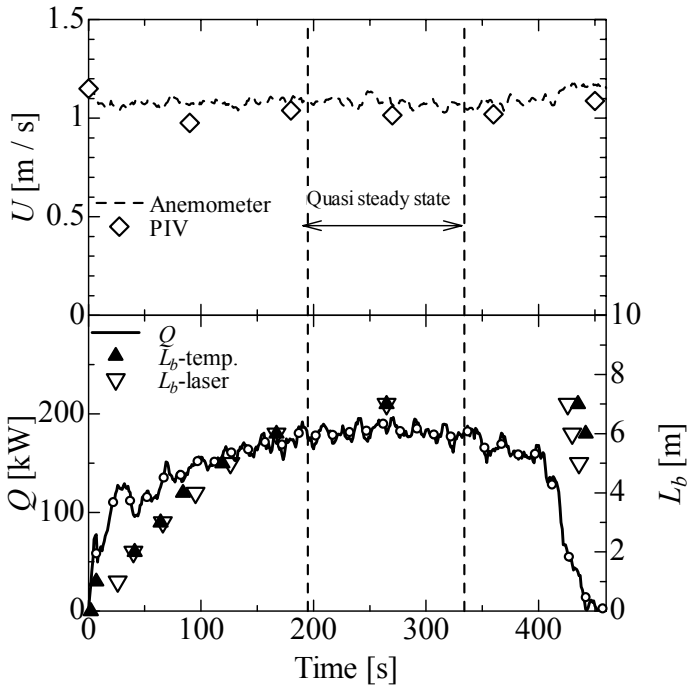

Fig. 3 Time curves of the heat release rate Q, ventilation velocity U, and backlayering distance L_b, in the case of a burning area of $A_f = 0.15$ m^2

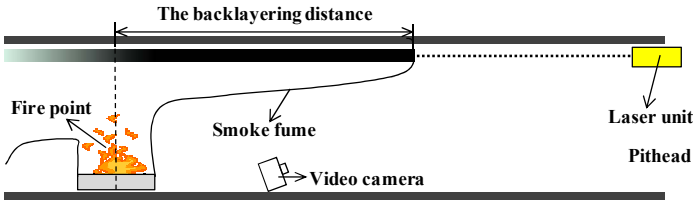

Fig. 4 Measurement of the backlayering distance using the laser beam

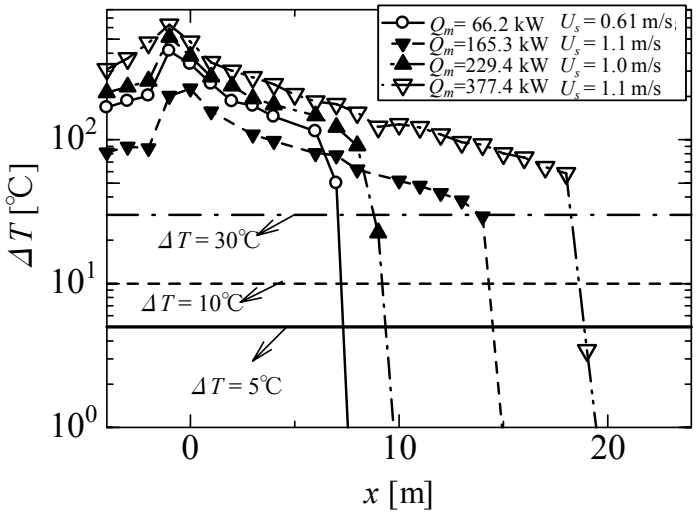

Fig. 5 Definition of the tip position of the thermal fumes based on temperature rise: δT = 5, 10, and 30 K

4. Backlayering characteristics of thermal fumes

4.1 Formula for calculating the backlayering distance

Figure 6 shows the relationship between the average velocity of the longitudinal ventilation on the horizontal axis and the backlayering distance on the vertical axis in the four cases of the average heat release rate. The backlayering distance decreases rapidly as the average longitudinal ventilation velocity increases in all cases.

Kunikane et al. conducted a numerical simulation of a fire in a tunnel with a large cross section by using computational fluid dynamics. Under constant conditions of the average heat release rate, an empirical formula between the backlayering distance and the average longitudinal velocity was developed by Kunikane et al. as Eq. (1). The constants a and b in the equation were calculated by the least squares method from the results of the numerical simulation. However, the equation has insufficient generality because the heat release rate of the fire is not taken into consideration.

$$L_b = \frac{a}{U_s} - b \tag{1}$$

Calculation formulas for the backlayering distance including the heat release rate of the fire have been developed by several researchers. Thomas[15] indicated that the dimensionless backlayering distance L_b/H is a function of the combined parameter Q^*/Fr^3. The parameters Q^* and Fr are the dimensionless heat release rate of a fire and the Froude number based on longitudinal ventilation velocity and tunnel height, respectively. This combined parameter Q^*/Fr^3 is the governing parameter of a backlayering phenomenon and indicates the ratio of

the buoyancy of thermal fumes to the inertial force by longitudinal ventilation wind in a tunnel.

Vantelon et al.[11] conducted an experimental tunnel fire using a heat-resistant glass model tunnel with a semicircular cross section. The experimental conditions are shown in Table 1. Based on the experimental results, Vantelon et al. developed a formula for the dimensionless backlayering distance as Eq. (2) with the exponent n set to 0.3.

$$\frac{L_b}{H} = c\left(\frac{Q^*}{Fr^3}\right)^n \tag{2}$$

Saito et al.[12] and Yamada et al.[5] conducted tunnel fire experiments using ceramic fiberboard model tunnels with a rectangular cross-section for which the aspect ratio was unity. The experimental conditions are shown in Table 1. Saito et al. indicated that the exponent n in Eq. (2) gradually approached 0.3 as the parameter Q^*/Fr^3 increased. Yamada et al. indicated that the exponent n in the equation was one-third in the range of $L_b/H > 10$, and the value of n did not depend on the heat release rate of the fire. Moreover, the parameter c in Eq. (2) ranged from 0.6 to 2.2. However, the equation has the following disadvantage: The dimensionless backlayering distance becomes zero when the Froude number is infinity or the dimensionless heat release rate is zero. In actuality, the dimensionless backlayering distance becomes zero when the Froude number is a finite value or the dimensionless heat release rate is higher than zero. Therefore, the equation is not able to calculate the backlayering distance with sufficient accuracy when the dimensionless backlayering distance approaches zero.

In this study, we proposed a new equation to calculate the backlayering distance. Equation (3) includes new parameters d and e. Parameter d has the same role as parameter c in Eq. (2). Parameter e is introduced to calculate the backlayering distance with sufficient accuracy by using a finite Froude number or a dimensionless heat release rate that is higher than zero when the dimensionless backlayering distance approaches zero.

$$\frac{L_b}{H} = d\left(\frac{Q^*}{Fr^3}\right)^{1/3} - e = d\left(\frac{Q^{*1/3}}{Fr}\right) - e \tag{3}$$

Figure 7 shows the relationship between the dimensionless backlayering distance and the combined parameter $Q^{*1/3}/Fr$. The dimensionless backlayering distance is approximately proportional to the combined parameter in the four cases of the dimensionless heat release rate. The constants d and e in Eq. (3) were calculated by using the least squares method from the measured data except the dimensionless heat release rate $Q_m^* = 0.182$. As a result, the constants were $d = 20$ and $e = 18$, respectively. The solid line calculated by using these constants is shown in Fig. 7 and is in accord with the experimental results in the case of $Q_m^* = 0.0316$, 0.0775, and 0.111, respectively. In the case of the maximum heat release rate $Q_m^* = 0.182$, compared with the heat release rate Q_m^* ranging from 0.0316 to 0.111, the proportionality coefficient of L_b/H to $Q^{*1/3}/Fr$ is small because the flames of the fire source reached the tunnel ceiling. As a result, the temperature under the ceiling above the fire source was nearly the maximum value because the average temperature of the flames was a constant of about 800°C. In this case, the temperature rise under the ceiling was not proportional to the increase of the heat release rate. As a result, the proportionality coefficient of L_b/H to $Q^{*1/3}/Fr$ became small. The flames of the fire source did not reach the ceiling in the case of the heat release rate Q_m^* ranging from 0.0316 to 0.111. The temperature rise under the ceiling above the fire source increased as the heat release rate increased. As a result, the proportionality coefficient of L_b/H to $Q^{*1/3}/Fr$ was larger than that of the case of the maximum heat release rate $Q_m^* = 0.182$. Equation (3) derived in the present study can be used to determine the backlayering distance in the dimensionless heat release rate ranging from 0.0316 to 0.111.

The chained line representing Vantelon et al.'s Eq. (2), in which the exponent n was set

to 0.3, is also shown in Fig. 7. The chained line is not in agreement with our experimental data. Hu et al. developed the semiempirical Eq. (4) to calculate the backlayering distance in a tunnel fire. The equation is based on Thomas' theory, according to which the backlayering distance depends on the buoyancy of the thermal fumes and the inertial force by the longitudinal ventilation wind, and the empirical relationship of temperature in a tunnel fire.

$$L_b = \ln\left[K_2 \cdot \left(\frac{C_k H}{U_s^2}\right)\right] \Big/ 0.019, \quad K_2 = g \cdot \gamma \left[\left(\frac{As \cdot Q^*}{Fr}\right)^{2/3}\right]^{\varepsilon} \tag{4}$$

Figure 7 also shows the double-dashed chained line representing Eq. (4). The constant C_k in the equation ranges from 0.2 to 0.4. Here, we used 0.3 as the constant C_k in Eq. (4). The parameters γ and ε are decided by the parameter $(A_s Q^*/Fr)^{2/3}$ as follows:

$$\begin{aligned} &\gamma = 1.77, \quad \varepsilon = \frac{6}{5}, \quad \left(\frac{A_s Q^*}{Fr}\right)^{\frac{2}{3}} < 1.35 \\ &\gamma = 2.54, \quad \varepsilon = 0, \quad \left(\frac{A_s Q^*}{Fr}\right)^{\frac{2}{3}} \geq 1.35 \end{aligned} \tag{5}$$

The double-dashed chained line representing Eq. (4) is in agreement with the black circle in the case of $Q_m^* = 0.0316$ as shown in Fig. 7. Furthermore, Eq. (4) is in agreement with our newly proposed Eq. (3). The parameters d and e in Eq. (3) were determined based on the fire experiments using the large-scale model tunnel. Likewise, Hu et al. determined the parameters γ and ε of Eq. (4) based on the fire experiments of a full-scale tunnel: a two-lane horseshoe tunnel of 7.2 m in height, 10.8 m in width, and aspect ratio of 1.5. As a result, Eq. (3) and Eq. (4) are similar to each other, as shown in Fig. 7.

Figure 8 shows the relationship between Q_m^* and L_b/H when the Froude number is 0.319. The dimensionless backlayering distance increases as the dimensionless heat release rate increases. The dimensionless backlayering distances indicated by the solid line and the double-dashed chained line have a tendency to approach about 20 when the dimensionless heat release rate is in excess of 0.2. Moreover, the backlayering distance calculated by Hu et al.'s Eq. (4) is longer than that calculated by our newly proposed Eq. (3) in all ranges of Q_m^*. Equation (3) is in agreement with the black circle showing the experimental results over a range of the dimensionless heat release rate Q_m^* from 0.0316 to 0.111. However, both Eq. (3) and Eq. (4) overcalculate the backlayering distance when the dimensionless heat release rate is not less than 0.111. This is because the proportionality coefficient of L_b/H to $Q^{*1/3}/Fr$ becomes small when the heat release rate $Q_m^* = 0.182$, as shown in Fig. 7.

Table 1 Comparison of experimental conditions and dimensionless number

	Present	-	Vantelon[11]	Saito[12]	Yamada[5]	Lee[6], [13]	Roh[8]
Type	Model tunnel	Full-scale tunnel	Model tunnel	Model tunnel	Model tunnel	Model tunnel	Model tunnel
Section	Rectangular	Rectangular	Semicircular	Square	Square	Rectangular	Horseshoe
Height H [m]	1	5	0.15	0.3	0.3	0.4	0.4
Width B [m]	1.93	10	0.3	0.3	0.3	0.4	0.4
Sectional area A [m^2]	1.93	50	0.0353	0.09	0.09	0.16	0.143
Total length / H	41.4	-	20	72	72	26	25
Fire source upstream distance / H	32.1	-	10	36	36	18.5	13.3
Re	41000–110000	450000–1200000	1900–2200	5800–8300	3900–13000	8100–26000	18000–27000
Fr	0.19–0.53	0.19–0.53	0.16–0.21	0.175–0.25	0.12–0.40	0.19–0.34	0.22–0.85
Q^*_m	0.032–0.182	0.032–0.182	0.0218–0.0524	0.13	0.037–0.146	0.089	0.065–0.14
Fuel	n-Heptane	-	No data	Methanol	LPG	Ethanol	n-Heptane
Lower calorific value [MJ/kg]	44.56	-	-	19.86	50.2	26.89	44.56
Material (Near the fire source)	ALC	Concrete	Heat-resistant glass	Ceramic fiberboard	Ceramic fiberboard	Acrylic resin (Gypsum board)	Acrylic resin (Steel)
Bi (l = H)	41–118	22–66	0.88–2.7	7.9–64	7.9–64	19–55	19–55
Fo (l = H)	6.4×10^{-8}	2.4×10^{-8}	3.7×10^{-6}–4.0×10^{-6}	2.5×10^{-6}–8.7×10^{-7}	2.5×10^{-6}–8.7×10^{-7}	1.2×10^{-7}	1.2×10^{-7}

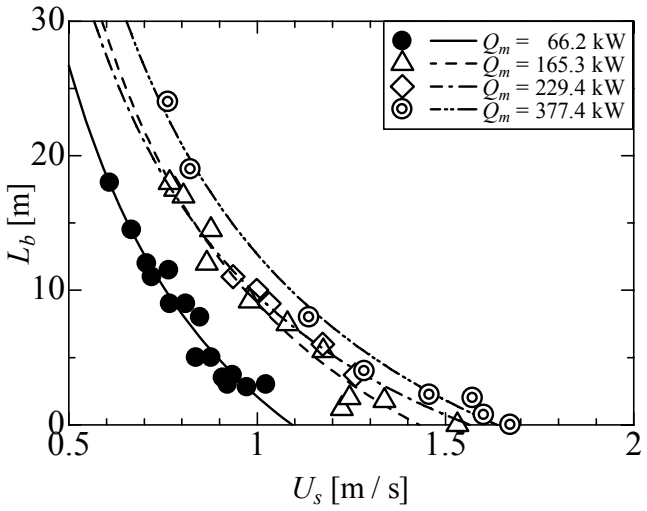

Fig. 6 Relationship between the average longitudinal velocity U_s and the backlayering distance L_b in four cases of average heat release rate Q_m. The symbols indicate the following: black circles, 66.2 kW; white triangles, 165.3 kW; white diamonds, 229.4 kW; double circles, 377.4 kW. The solid line, dashed line, chained line, and double-dashed chained line were drawn by using Eq. (1), respectively. The constants of Eq. (1) were calculated from the experimental data, using the least squares method.

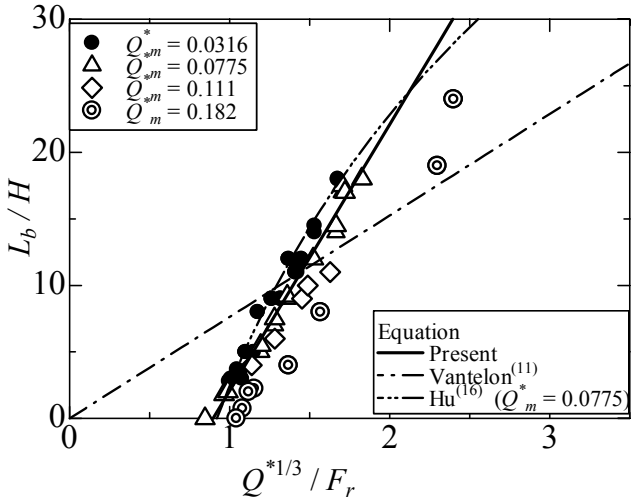

Fig. 7 Relationship between L_b/H and $Q^{*1/3}/Fr$. Four types of symbols show the dimensionless average heat release rate Q^*_m in the range from 0.0316 to 0.182. The solid line, chained line, and double-dashed chained line represent Eqs. (3), (2), and (4), respectively.

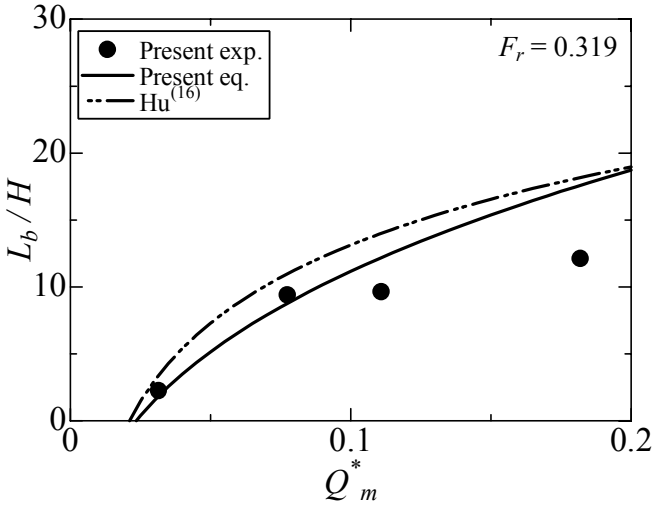

Fig. 8 Relationship between Q^*_m and L_b/H when Fr = 0.319. The solid line, double-dashed chained line, and black circles represent our newly proposed Eq. (3), Hu et al.'s Eq. (4), and the experimental results calculated from Fig. 7, respectively.

4.2 Comparison with previous work

Figure 9 shows the relationship between the dimensionless backlayering distance L_b/H and the combined parameter $Q^{*1/3}/Fr$, which is the governing parameter of the backlayering phenomenon, in the present study and in previous work by other researchers. A tunnel cross section of any shape was used in the previous work. Table 1 shows the experimental conditions of the present study and previous work, and the dimensionless parameters of the Froude number Fr, Reynolds number Re, dimensionless average heat release rate Q^*_m, Biot number Bi, and Fourier number Fo. As in the case of the solid line indicating our study, the dimensionless backlayering distances of the previous work are proportional to the combined parameter $Q^{*1/3}/Fr$ regardless of the shape or aspect ratio of the tunnel cross section, as shown in Fig. 9. However, the value of the proportionality constants of the previous studies is not in agreement with that of our study.

The plots of down-pointing double triangles in Fig. 9 show the results by Vantelon et al.

The plot data indicates that the constant of proportionality of the backlayering distance to the combined parameter $Q^{*1/3}/Fr$ was especially smaller than that of other researchers. In other words, the backlayering distance was shorter in the results of Vantelon et al. compared to the other researchers under the same value for the combined parameter $Q^{*1/3}/Fr$. The reason for this is as follows: The model tunnel made by Vantelon et al. was especially small in comparison with that made by other researchers, as shown in Table 1. The Reynolds number based on the tunnel height and the longitudinal velocity inside the model tunnel was about 2000. In this case, the flow regime inside the tunnel became almost laminar. Furthermore, the Fourier number *Fo* and Biot number *Bi* were considerably greater and smaller than those of the other tunnels, respectively, because the material of the tunnel wall was heat-resistant glass with high thermal conductivity. The characteristics of heat absorption through the wall were very different from those of a full-scale tunnel. The dimensionless average heat release rate Q^*_m in the range from 0.0218 to 0.0524 was smaller than that of the other experiments. In the case of the model tunnel made by Vantelon et al., the length from the fire source to the tunnel opening was only ten times the height of the model tunnel. The backlayering distance in the fire experiment was more than five times the height of the model tunnel. The length of the model tunnel was too short to be used in a backlayering distance experiment. The tunnel opening affected the experimental results because the entrance length for the longitudinal ventilation wind was too short.

The experimental data by Saito et al. is shown as the plots of white circles in Fig. 9. In their model tunnel, the length from the fire source to the tunnel opening was 36 times the height of the model tunnel, which was long enough to conduct an experiment on backlayering distance. The tunnel opening did not affect the experimental results. The proportionality coefficient of the backlayering distance to the combined parameter $Q^{*1/3}/Fr$ by Saito et al. was similar to that by Vantelon et al., because the Reynolds numbers of the flow in the tunnel were similar. Furthermore, the Fourier number of the wall of the model tunnel made of ceramic fiberboard was greater than that of a full-scale tunnel made of concrete, so the heat conductivity of the wall of the model tunnel was greater. The measurement accuracy in the research by Saito et al. was lower than that of the other researchers because the distance between the installed thermocouples under the tunnel ceiling was too large for accurate measurement of the backlayering distance. Furthermore, the velocity of the longitudinal ventilation was only present in four cases.

The plots of white squares in Fig. 9 show the experimental data by Lee et al. and those of the up-pointing double triangles and black triangles show the data by Yamada et al. The proportionality coefficients calculated from the data of the backlayering distance measured by Lee et al. and Yamada et al. were smaller than that of the present study. Therefore, the backlayering distance was shorter than that of the present study for the same value of the combined parameter $Q^{*1/3}/Fr$. Similar to the model tunnel of Vantelon et al., the Fourier number *Fo* of the wall of the model tunnel made of ceramic fiberboard or acrylic resin was greater than that of a full-scale tunnel made of concrete, and the heat flux through the wall of the model tunnel was greater. As a result, the backlayering distance became short. Furthermore, when the backlayering distance was zero, the value of the combined parameter $Q^{*1/3}/Fr$ was greater than that of the present study, because the aspect ratio of the cross-sectional shape of the model tunnel was different from that of our model tunnel. The aspect ratio of the model tunnel introduced by Lee et al. and Yamada et al. was unity; that of the model tunnel in the present study was 2.0. The backlayering distance in the present study (A_s = 2.0) was longer than that in the previous studies by the other researchers (A_s = 1.0) under the same conditions of heat release rate and velocity of longitudinal ventilation, as shown in Fig. 9. Furthermore, the critical velocity and critical Froude number in the present study (A_s = 2.0) were larger than in the previous studies (A_s = 1.0) under the same conditions of heat release rate, as shown in Fig. 9. Namely, the backlayering phenomenon

against the longitudinal ventilation wind was easily generated in a tunnel fire when the cross-sectional shape of the tunnel had a large aspect ratio.

The experimental data by Roh et al. is shown as plots of black down-pointing triangles in Fig. 9. The test range of the backlayering distance of their fire experiment was smaller than that applied by other researchers, because Roh et al. investigated not the backlayering distance but the critical velocity. The value of the combined parameter $Q^{*1/3}/Fr$ when the backlayering distance was zero, was close to that of combined parameter $Q^{*1/3}/Fr$ in the present study. The cross-sectional shape of the model tunnel made by Roe et al. was a horseshoe, which easily generated the backlayering phenomenon, similar to our tunnel with a large aspect ratio.

The experimental conditions of the present study were compared with those of the previous studies by using the data shown in Table 1. It is important to achieve completely turbulent flow in a model tunnel as well as a full-scale tunnel in the case of a model experiment. The model tunnel in this study was at least three times larger than that in other studies, as shown in Table 1. Therefore, the Reynolds number *Re* of the ventilation flow in the model tunnel was 40,000 or more, and completely turbulent flow was achieved. Furthermore, the Biot number *Bi* and Fourier number *Fo* of our model tunnel made of autoclaved lightweight aerated concrete (ALC) panels were close to the values of a full-scale tunnel made of concrete. The length from the fire source to the tunnel opening was 32 times the height of the model tunnel, which was long enough to conduct an experiment on the backlayering distance in a tunnel fire; the tunnel opening did not affect our experimental results. Therefore, we concluded that our experimental results were more accurate than those of other researchers.

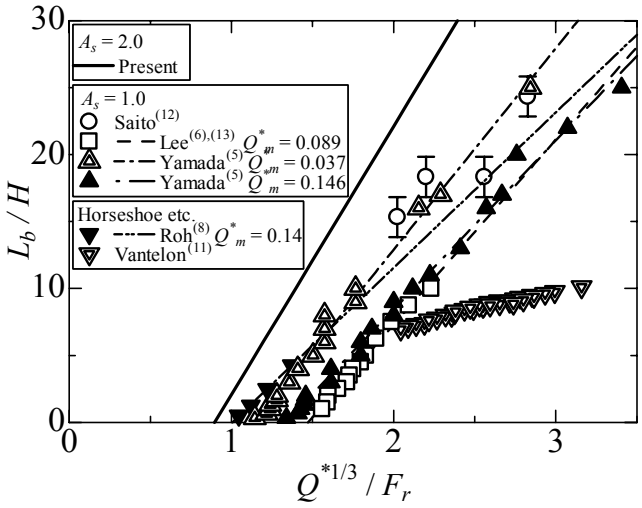

Fig. 9 Relationship between L_b/H and $Q^{*1/3}/Fr$. The comparison between the present study and previous work by Saito et al., Lee et al., and Yamada et al. using a model tunnel with a rectangular cross section of aspect ratio unity, by Roh et al. using a model tunnel with a horseshoe-shape cross section, and by Vantelon et al. using a model tunnel with a semicircular cross section.

4.3 Critical velocity

Substituting $L_b = 0$ into Eq. (3) yields Eq. (6) showing the critical Froude number Fr_c, which is defined by using the critical velocity of the longitudinal ventilation.

$$Fr_c = \frac{d}{e} Q^{*\frac{1}{3}} \tag{6}$$

Figure 10 shows the relationship between the dimensionless average heat release rate Q^*_m and the critical Froude number Fr_c. Critical velocity in a tunnel fire has been the

subject of extensive research for many years. Figure 10 includes the data plots determined by our study and that of the other researchers and the dashed line was calculated by using the theoretical formula derived by Thomas. The solid circles showing the critical Froude number calculated from the data of the present study increase in the dimensionless average heat release rate range of 0.0316 to 0.111. This trend was in agreement with the theoretical formula (dashed line) by Thomas and Eq. (6) derived in the present study. However, the solid circle showing the critical Froude number was not in agreement with the theoretical formula (dashed line) by Thomas and Eq. (6) in the dimensionless heat release rate Q^*_m exceeding 0.111, where the solid circle shows that the critical Froude number approaches about 0.5. Equation (6) had the ability to calculate the critical velocity in the dimensionless heat release rate ranging from 0.0316 to 0.111.

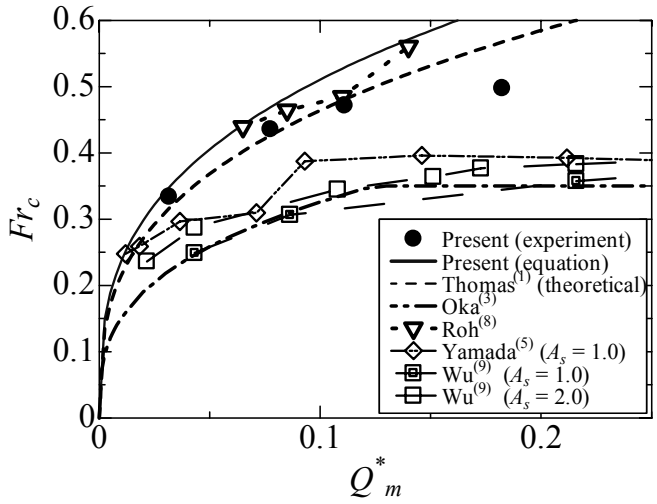

Fig. 10 Relationship between Q^*_m and Fr_c. The solid line and dashed line are drawn by using Eq. (6) and the theoretical formula derived by Thomas, respectively; the solid circles show the experimental data of the present study; the data of other researchers is indicated by a number of different symbols.

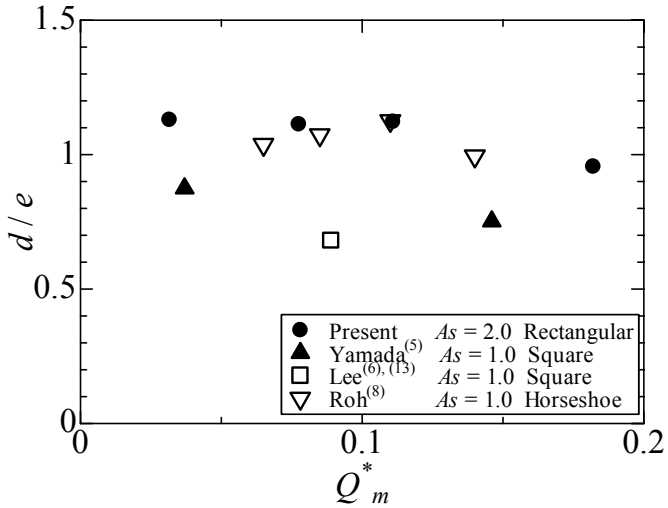

Fig. 11 Relationship between Q^* m and d/e

When the dimensionless heat release rate Q^*_m was the same, the critical Froude number of the present study was greater than that of the other studies. In the tunnel fire experiments conducted by other researchers, the characteristics of heat conduction inside the wall of the tunnel and the heat transfer from thermal fumes to the wall differed between the

model-scale tunnel of the present study and a full-scale tunnel. Namely, the Biot number and the Fourier number were different from those of a full-scale tunnel. Therefore, the heat absorption increased from the thermal fumes to the wall of the tunnel. As a result, the critical velocity and critical Froude number measured by the other researchers decreased compared to those in the present study, excluding the results obtained by Roh et al. The thermal characteristics of the wall of the tunnel made by Roh et al. were different compared to that of a full-scale tunnel. However, the cross-sectional shape of their tunnel was a horseshoe, which easily generated the backlayering phenomenon, as shown in Fig. 9. As a result, the critical Froude number by Roh et al. was greater than that obtained by other researchers. The critical Froude number approaches a maximum value in the case of almost all experimental results when the dimensionless heat release rate Q^*_m is greater than 0.1, even if the cross-sectional shape is different.

Figure 11 shows the relationship between the parameter d/e in Eq. (6) and the dimensionless heat release rate Q^*_m. In addition to our data, the parameter d/e was also calculated from the experimental results of other researchers. The parameter d/e indicates the relationship between the critical Froude number and the dimensionless heat release rate. When Q^*_m = 0.0316, 0.0775, and 0.111 in our results, the parameter d/e is almost the same. When Q^*_m = 0.182, however, the parameter d/e decreases. When the longitudinal ventilation velocity was the same, which was the condition under a constant Froude number, the growth rate of the dimensionless backlayering distance decreased when the dimensionless heat release rate Q^*_m was greater than 0.111. This was in agreement with the tendency of the growth rate of the backlayering distance as shown in Fig. 8. The value of the parameter d/e of the results by Yamada et al. and Lee et al. was smaller than that of our results. The reason for this is that the aspect ratio of the cross-sectional shape of the model tunnel made by Yamada et al. was 1.0 (our model tunnel is As = 2.0). The value of the parameter d/e of the results by Roh et al. was close to that of our results, because the cross-sectional shape of their model tunnel was a horseshoe.

5. Conclusions

Tunnel fire experiments were conducted using a large-scale model tunnel to produce completely turbulent flow in the tunnel and considering the heat transfer characteristics of the tunnel wall. The main results of this research are as follows.

1. Equation (3), which is used to calculate the backlayering distance, is proposed as a function of the dimensionless heat release rate Q^*_m and the Froude number Fr.
2. Equation (6), which is used to calculate the critical velocity, is proposed as a function of the dimensionless heat release rate Q^*_m.
3. The growth rate of the dimensionless backlayering distance decreases when the dimensionless heat release rate Q^*_m is greater than 0.111.
4. The backlayering distance in which the aspect ratio of the model tunnel is 2.0, is longer than when the aspect ratio of the model tunnel is unity, under the same conditions of heat release rate and velocity of longitudinal ventilation.
5. Equation (4) developed by Hu et al. is in agreement with our newly proposed Eq. (3).

References

(1) Thomas, P.H., The Movement of Smoke in Horizontal Passages against an Air Flow, *Fire Research Note*, No. 723, (1968), Fire Research Station.

(2) Danziger, N.H. and Kennedy, W.D., Longitudinal Ventilation Analysis for the Glenwood Canyon Tunnels, *Proceedings of the 4th International Symposium on Aerodynamics and Ventilation of Vehicle Tunnels*, (1982), pp. 169-186.

(3) Oka, Y. and Atkinson, G.T., Control of Smoke Flow in Tunnel Fires, *Fire Safety Journal*, Vol. 25, (1995), pp. 305-322.
(4) Mizutani, T., Horiuchi, K., et al., Report on tunnel fire test – the tunnel fire test for longitudinal ventilation, *Technical Note of the Public Works Research Institute*, No. 1876, (1982).
(5) Yamada, T., Watanabe, Y., Matsushima, S., Oka, Y., Kurioka, H., Kuwana, H. and Satoh, H., Ventilation Criteria for Preventing Backing Layer of Smoke in Case of Tunnel Fire, *Report of National Research Institute of Fire and Disaster*, No. 83 (1997), pp. 37-46.
(6) Lee, S.R. and Ryou, H.S., An Experimental Study of the Effect of the Aspect Ratio on the Critical Velocity in Longitudinal Ventilation Tunnel Fires, *Journal of Fire Sciences*, Vol. 23, (2005), pp. 119-138.
(7) Lannermark, A. and Ingason, H., Fire Spread and Flame Length in Large-Scale Tunnel Fires, *Fire Technology*, Vol. 42, No. 4, (2006), pp. 283-302.
(8) Roh, J.S., Seung, H. Y., Hong, S.R., Myong, O.Y. and Youn, T.J., An experimental study on the effect of ventilation velocity on burning rate in tunnel fires – heptane pool case, *Building and Environment*, 43, (2008), pp. 1225-1231.
(9) Wu, Y. and Bakar, M.Z.A., Control of smoke flow in tunnel fires using longitudinal ventilation systems – a study of the critical velocity, *Fire Safety Journal*, Vol. 35, (2000), pp. 363-390.
(10) Wang, Q., Kawabata, N. and Ishikawa, T., Evaluation of Critical Velocity Employed to Prevent the Backlayering of Thermal Fume during Tunnel Fires, *Proc. of Int. Conf. on ACFD*, Oct., (2000), pp. 404-411.
(11) Vantelon, J.P., Guelzim, A., Quach, D. and Son, D.K., Investigation of Fire-Induced Smoke Movement in Tunnels and Stations: An Application to the Paris Metro, *Proceedings of the Third International Symposium on Fire Safety Science*, (1991), pp. 907-918.
(12) Saito, N., Sekizawa, A., Yamada, T., Yanai, E., Watanabe, Y. and Miyazaki, S., Study Report on Fire Performance in Special Space of Use of Underground Space, *Fire Defence Research Datum*, No. 29 (1994).
(13) Lee, S.R. and Ryou, S.H., A numerical study on smoke movement in longitudinal ventilation tunnel fires for different aspect ratio, *Building and Environment*, 41, (2006), pp. 719-725.
(14) Kunikane, Y., Kawabata, N., Yamada, T. and Shimoda, A., Influence of Stationary Vehicles on Backlayering Characteristics of Fire Plume in a Large Cross Section Tunnel, *JSME International Journal*, Series B, Vol. 49, No. 3, (2006), pp. 594-600.
(15) Thomas, P.H., The movement of buoyant fluid against a stream and the venting of underground fires, *Fire Research Note*, No. 351, (1958), Fire Research Station.
(16) Hu, L.H., Huo, R. and Chow, W.K., Studies on buoyancy-driven back-layering flow in tunnel fires, *Experimental Thermal and Fluid Science*, 32, (2008), pp. 1468-1483.
(17) Fujita, K., Minehiro, T., Kawabata, N., Tanaka, F., Temperature Characteristics of Backlayering Thermal Fumes in a Tunnel Fire, *Transactions of the Japan Society of Mechanical Engineers*, Series B, Vol. 76, No. 768 (2010), pp. 1176-1183.
(18) Kikumoto, T., Kawabata, N., Maruyama, D. and Yamada, M., Model Tests on Fire Smoke Behavior in a Small Road Tunnel for Passenger Cars, *Journals of the Japan Society of Civil Engineers*, Division F, Vol. 63, No. 3 (2007), pp. 361-373.
(19) Kunikane, Y., Kawabata, N., Takekuni, K., and Shimoda, A., Heat Release Rate of Gasoline Pool Fire in Large Cross Sectional Tunnel, *Transactions of the Japan Society of Mechanical Engineers*, Series B, Vol. 69, No. 685 (2003), pp. 2044-2051.
(20) Sveen, J.K., An introduction to MatPIV v. 1.6.1, *Mechanics and Applied Mathematics*, No. 2 (2004).
(21) PIARC Committee on Road Tunnel Operations (C3.3), Systems and Equipment for Fire and Smoke Control in Road Tunnels (2007).